

On the convergence and sampling of randomized primal-dual algorithms and their application to parallel MRI reconstruction

Eric B Gutierrez, Claire Delplancke and Matthias J Ehrhardt

Department of Mathematical Sciences, University of Bath, BA2 7AY, UK

E-mail: ebgc20@bath.ac.uk, cd902@bath.ac.uk, M.Ehrhardt@bath.ac.uk

June 2022

Abstract. Stochastic Primal-Dual Hybrid Gradient (SPDHG) is an algorithm to efficiently solve a wide class of nonsmooth large-scale optimization problems. In this paper we contribute to its theoretical foundations and prove its almost sure convergence for convex but neither necessarily strongly convex nor smooth functionals. We also prove its convergence for any sampling. In addition, we study SPDHG for parallel Magnetic Resonance Imaging reconstruction, where data from different coils are randomly selected at each iteration. We apply SPDHG using a wide range of random sampling methods and compare its performance across a range of settings, including mini-batch size and step size parameters. We show that the sampling can significantly affect the convergence speed of SPDHG and for many cases an optimal sampling can be identified.

Keywords: Inverse Problems, Parallel MRI, Primal-dual, Stochastic, Optimization

1. Introduction

Inverse problems can be solved using variational regularization, generally presented as an optimization problem. In fields such as imaging, data science or machine learning, optimization challenges are generally formulated as the convex minimization problem

$$\hat{x} \in \arg \min_{x \in X} \sum_{i=1}^n f_i(A_i x) + g(x) \quad (1)$$

where $f_i : Y_i \rightarrow \mathbb{R} \cup \{\infty\}$ and $g : X \rightarrow \mathbb{R} \cup \{\infty\}$ are convex functionals, and $A_i : X \rightarrow Y_i$ are linear and bounded operators between real Hilbert spaces.

Many active areas of research exists within this framework, with problems such as regularized risk minimization [5, 7, 36, 39], heavily-constrained optimization [15, 26] or total variation regularization image reconstruction [33]. Within the context of image reconstruction, examples of problems in the form of (1) are image denoising [10], PET

reconstruction [13] and, most relevant to the present paper, parallel Magnetic Resonance Imaging (MRI) reconstruction [17, 20, 29].

Problem (1) makes no assumptions on the differentiability of the convex functionals f_i, g . In general, if these functionals are not smooth then many classical approaches such as gradient descent are not applicable [10]. In contrast, primal-dual methods are able to solve (1) even for non-smooth functionals. When f_i, g are convex, proper and lower-semicontinuous, the *saddle point problem* for (1) is

$$\hat{x}, \hat{y} \in \arg \min_{x \in X} \max_{y \in Y} \sum_{i=1}^n \langle A_i x, y_i \rangle - f_i^*(y_i) + g(x) \quad (2)$$

where f_i^* is the *convex conjugate* of f_i and $Y = \Pi_{i=1}^n Y_i$. We refer to a solution of (2) as a *saddle point*.

A well-known primal-dual method is the Primal-Dual Hybrid Gradient algorithm (PDHG) [9, 14, 27]. While PDHG is proven to converge to a saddle point, its iterations can be costly for large-scale problems, e.g. when $n \gg 1$ [8]. A random primal-dual method, the Stochastic Primal-Dual Hybrid Gradient algorithm (SPDHG) was proposed recently by Chambolle et al. [8]. Its main difference over PDHG is that it reduces the per-iteration computational cost by randomly sampling the dual variable, i.e. only a random subset of the dual variable gets updated at every iteration. In [8], it is shown that SPDHG offers significantly better performance than the deterministic PDHG for large-scale problems [13, 35]. Examples of other random primal-dual algorithms can be found in [16, 18, 23, 39].

In the original paper [8], SPDHG's almost sure convergence is proven for strongly convex functionals f_i^*, g . Later, for the special case of serial sampling, Alacaoglu et al. proved SPDHG's almost sure convergence for arbitrary convex functionals in finite-dimensional Hilbert spaces [2]. An alternative proof can also be found in [19].

In this paper we complete the gap on the convergence theory of SPDHG and prove its almost sure convergence for any convex functionals on Hilbert spaces and for any arbitrary random sampling. This generalizes the existing convergence results in two ways. The first is the extension into Hilbert spaces, which extends the usefulness of SPDHG into infinite-dimensional function spaces that are important in many areas such as quantum mechanics, functional analysis and partial differential equations [34]. While further generalizations of PDHG into Banach spaces have also been studied [21], for simplicity of the argument we restrict ourselves to arbitrary dimensional Hilbert spaces.

The second generalization is the convergence of SPDHG for any arbitrary sampling. The proofs for convergence presented in both [2] and [19] rely heavily on the assumption that SPDHG uses serial sampling for choosing the random updates. In this paper we present a proof of convergence for any sampling, and we propose adequate step size conditions for several specific examples of random samplings.

Furthermore, as a novel application of SPDHG we perform parallel MRI reconstruction on real MRI data. MRI reconstruction describes an inverse problem with

a data structure that can be naturally randomized, and serves as an ideal candidate to compare performance of SPDHG under different random samplings. Our numerical examples show that information on the forward problem can help identify an optimal sampling as well as optimal step size parameters.

2. Stochastic Primal-Dual Hybrid Gradient

SPDHG is the result of randomizing the deterministic PDHG algorithm. PDHG with dual extrapolation [9, 28] is given by

$$\begin{aligned} x^{k+1} &= \text{prox}_{\tau g}(x^k - \tau A^* \bar{y}^k) \\ y_i^{k+1} &= \text{prox}_{\sigma_i f_i^*}(y_i^k + \sigma_i A_i x^{k+1}) \quad \text{for } i \in \{1, \dots, n\} \\ \bar{y}^{k+1} &= y^{k+1} + \theta(y^{k+1} - y^k) \end{aligned} \quad (3)$$

where $\tau, \sigma_i > 0$ are step-size parameters, \bar{y}^{k+1} is an extrapolation with parameter $\theta \in [0, 1]$, operator $A^* : Y \rightarrow X$ is $A^*y = \sum_i A_i^* y_i$, and the *proximity operator* [3] is

$$\text{prox}_h(v) := \arg \min_u \frac{\|v - u\|^2}{2} + h(u).$$

This method is proven to converge for $\theta = 1$ and step size condition $\tau \sigma_i \|A\|^2 < 1$ for every $i \in \{1, \dots, n\}$, for any convex functionals g, f_i^* [9].

SPDHG, in contrast, reduces the cost of (3) by updating only a random subset of the coordinates $(y_i)_{i=1}^n$. This means, at every iteration k , a subset $\mathbb{S}^k \subset \{1, \dots, n\}$ is chosen at random and only the variables y_i^{k+1} for $i \in \mathbb{S}^k$ are updated, while the rest remain unchanged:

$$y_i^{k+1} = \begin{cases} \text{prox}_{\sigma_i f_i^*}(y_i^k + \sigma_i A_i x^{k+1}) & \text{if } i \in \mathbb{S}^k \\ y_i^k & \text{else.} \end{cases}$$

We assume the random variables \mathbb{S}^k are independent and identically distributed. Furthermore, the sampling must be proper, i.e. it must satisfy

$$p_i := \mathbb{P}(i \in \mathbb{S}^k) > 0 \quad \text{for every } i \in \{1, \dots, n\}, \quad (4)$$

meaning the probability p_i of updating any coordinate i must be nonzero. The complete SPDHG algorithm is given in Algorithm 1.

In order to minimize the number of linear operations, the auxiliary variable z^k stores the current value of A^*y^k , so that only the operators A_i^* for $i \in \mathbb{S}^k$ need to be evaluated at each iteration. Similarly, \bar{z}^{k+1} represents the extrapolation

$$\bar{z}^{k+1} = A^*y^{k+1} + A^*Q(y^{k+1} - y^k)$$

where $Q : Y \rightarrow Y$ is the operator defined by $(Qy)_i = p_i^{-1}y_i$. We will often refer to the fact that Q is symmetric and positive definite.

For serial sampling, where only one coordinate is selected at every iteration, i.e. $|\mathbb{S}^k| = 1$ for every k , SPDHG takes the form of Algorithm 2, which is the special case of Algorithm 1 where we set $\mathbb{S}^k = \{j^k\}$ and only $y_{j^k}^{k+1}$ and $\delta = \delta_{j^k}$ are activated at each iteration k .

Algorithm 1 SPDHG

Choose $x^0 \in X$ and $y^0 \in Y$.
Set $z^0 = \bar{z}^0 = A^*y^0$.
for $k \geq 0$ **do**
 select $\mathbb{S}^k \subset \{1, \dots, n\}$ at random
 $x^{k+1} = \text{prox}_{\tau g}(x^k - \tau \bar{z}^k)$
 $y_i^{k+1} = \begin{cases} \text{prox}_{\sigma_i f_i^*}(y_i^k + \sigma_i A_i x^{k+1}) & \text{if } i \in \mathbb{S}^k \\ y_i^k & \text{else} \end{cases}$
 $\delta_i = A_i^*(y_i^{k+1} - y_i^k)$ for all $i \in \mathbb{S}^k$
 $z^{k+1} = z^k + \sum_{i \in \mathbb{S}^k} \delta_i$
 $\bar{z}^{k+1} = z^{k+1} + \theta \sum_{i \in \mathbb{S}^k} p_i^{-1} \delta_i$
end for

Algorithm 2 SPDHG for serial sampling

Choose $x^0 \in X$ and $y^0 \in Y$.
Set $z^0 = \bar{z}^0 = A^*y^0$.
for $k \geq 0$ **do**
 select $j^k \in \{1, \dots, n\}$ at random
 $x^{k+1} = \text{prox}_{\tau g}(x^k - \tau \bar{z}^k)$
 $y_i^{k+1} = \begin{cases} \text{prox}_{\sigma_i f_i^*}(y_i^k + \sigma_i A_i x^{k+1}) & \text{if } i = j^k \\ y_i^k & \text{else} \end{cases}$
 $\delta = A_{j^k}^*(y_{j^k}^{k+1} - y_{j^k}^k)$
 $z^{k+1} = z^k + \delta$
 $\bar{z}^{k+1} = z^{k+1} + \theta p_{j^k}^{-1} \delta$
end for

3. Convergence analysis

In this section we state the almost sure convergence of SPDHG to a saddle point of the primal-dual problem (2), as well as the conditions under which this is true. This result extends the usefulness of SPDHG by generalizing its existing convergence theory into any arbitrary sampling, as well as into Hilbert spaces.

Hilbert spaces are specially relevant in the context of image processing, since images can often be modelled by square-integrable functions on the plane [6], which constitutes an infinite-dimensional space. Examples of imaging problems in Hilbert spaces are wavelet shrinkage denoising, where the challenge consists in finding a sparse representation of the image in the infinite basis [37]; or super-resolution imaging, which describes the inverse problem of finding the square-integrable function that best approximates a set of low-resolution images [11].

Optimal step size parameters for SPDHG are explained in Section 4. Different applications of the algorithm are illustrated in Section 5.

Assumption 1. We assume the following to hold:

- (i) The Hilbert spaces X, Y are real and separable.
- (ii) The set of solutions to (2) is nonempty.
- (iii) The functionals g, f_i are convex, proper and lower-semicontinuous.
- (iv) The proximity operators $\text{prox}_{\tau g}, \text{prox}_{\sigma_i f_i^*}$ are weakly sequentially continuous.

Assumptions (i), (ii) and (iii) are as in the original SPDHG result ([8], Theorem 4.3), and Assumption (ii) is further discussed in [2]. Assumption (iv) is always satisfied in finite dimensions, since the proximity operator prox_h is continuous for any convex, proper and lower-semicontinuous functional h ([3], Proposition 12.28).

In general, a function T is *weakly sequentially continuous* if, for every sequence $(v^k)_{k \in \mathbb{N}}$ converging weakly to v , the sequence $(T(v^k))_{k \in \mathbb{N}}$ converges weakly to $T(v)$. For examples of separable sums of convex functions that satisfy Assumption (iv), see ([3], Proposition 24.12).

We recall that a (weak) *cluster point* of a sequence $(x^k)_{k \in \mathbb{N}}$ is any point \hat{x} such that there exists a subsequence $(x^{\ell_k})_{k \in \mathbb{N}}$ which converges (weakly) to \hat{x} . Furthermore, for a probability space denoted by $(\Omega, \mathcal{F}, \mathbb{P})$, we say a sequence $(x^k)_{k \in \mathbb{N}}$ converges (weakly) *almost surely* to \hat{x} if there exists $\Omega \in \mathcal{F}$ such that $\mathbb{P}(\Omega) = 1$ and $x^k(\omega) \rightarrow \hat{x}(\omega)$ (weakly) for every $\omega \in \Omega$. For brevity, we write *a.s.* instead of almost surely.

Additionally, in order to state the step size conditions, we use the following notation. For any subset $\mathcal{S} \subset \{1, \dots, n\}$, let $A_{\mathcal{S}} : X \rightarrow Y$ be given by

$$(A_{\mathcal{S}}x)_i := \begin{cases} A_i x & \text{if } i \in \mathcal{S} \\ 0 & \text{else} \end{cases}$$

with adjoint $A_{\mathcal{S}}^* y = \sum_{i \in \mathcal{S}} A_i^* y_i$.

Similarly, denote $C_i = \tau^{1/2} \sigma_i^{1/2} A_i$ for $i \in \{1, \dots, n\}$, with adjoints $C_i^* = \tau^{1/2} \sigma_i^{1/2} A_i^*$, and $C_{\mathcal{S}}$ and $C_{\mathcal{S}}^*$ defined accordingly as above. For any random sampling \mathbb{S} , we define the step size operator D as

$$D := Q \mathbb{E}(C_{\mathbb{S}} C_{\mathbb{S}}^*) Q. \quad (5)$$

Theorem 1 (Convergence of SPDHG). Let Assumption 1 be satisfied, $\theta = 1$ and

$$\|D\| < 1. \quad (6)$$

Then Algorithm 1 converges weakly a.s. to a solution of (2).

3.1. Step size condition

In the original paper of SPDHG [8], the authors describe the step size condition using *ESO parameters* [31]. While these conditions are equivalent, we prefer to use (6) because it offers a practical way to check the validity of the step-size parameters τ, σ_i by finding the eigenvalues of D . Moreover, from [31] we know $D : Y \rightarrow Y$ can be expressed as

$$D = \begin{pmatrix} D_{11} & \cdots & D_{1n} \\ \vdots & \ddots & \vdots \\ D_{n1} & \cdots & D_{nn} \end{pmatrix}, \quad D_{ij} = \frac{p_{ij}}{p_i p_j} C_i C_j^* \quad (7)$$

where $D_{ij} : Y_j \rightarrow Y_i$ and $p_{ij} = \mathbb{P}(i \in \mathbb{S}, j \in \mathbb{S})$. In contrast, ESO parameters are parameters v_1, \dots, v_n such that

$$\mathbb{E} \|C_{\mathbb{S}}^* z\|^2 \leq \sum_{i=1}^n p_i v_i \|z_i\|^2 \quad (8)$$

and the step size condition for SPDHG in [8] is

$$v_i < p_i \quad \text{for all } i \in \{1, \dots, n\}. \quad (9)$$

The following lemma shows this condition is equivalent to (6).

Lemma 1. *Let D be defined as in (5). Then $\|D\| < 1$ if and only if there exist ESO parameters v_i such that $v_i < p_i$ for $i \in \{1, \dots, n\}$.*

Proof. Let $\|D\| < 1$. Then

$$\mathbb{E} \|C_{\mathbb{S}}^* z\|^2 = \langle z, \mathbb{E}(C_{\mathbb{S}} C_{\mathbb{S}}^*) z \rangle = \langle Q^{-1} z, D Q^{-1} z \rangle \leq \|D\| \|Q^{-1} z\|^2 = \|D\| \sum_{i=1}^n p_i^2 \|z_i\|^2.$$

hence (8) and (9) are satisfied by choosing $v_i = \|D\| p_i$. Conversely, let v_i satisfy (8) and (9),

$$\langle D z, z \rangle = \langle \mathbb{E}(C_{\mathbb{S}} C_{\mathbb{S}}^*) Q z, Q z \rangle = \mathbb{E} \|C_{\mathbb{S}}^* Q z\|^2 \leq \sum_{i=1}^n p_i v_i \|p_i^{-1} z_i\|^2 < \sum_{i=1}^n p_i^2 \|p_i^{-1} z_i\|^2 = \|z\|^2$$

which proves $\|D\| < 1$. \square

Clearly, the step size parameters τ, σ_i that satisfy (6) are not unique. In particular, if we assume the step size parameters to be uniform, i.e. $\sigma_i = \sigma$ for all i , then we write $D = \tau \sigma Q \mathbb{E}(A_{\mathbb{S}} A_{\mathbb{S}}^*) Q$ and thus it suffices to choose τ, σ such that

$$\tau \sigma \|Q \mathbb{E}(A_{\mathbb{S}} A_{\mathbb{S}}^*) Q\| < 1. \quad (10)$$

In Section 4, we will see examples on how to find optimal step sizes that comply with this condition for specific types of random samplings.

3.2. Proof of Theorem 1

The two following propositions lay out the proof of Theorem 1. We use the notation $w = (x, y)$.

Proposition 1. *Let $\theta = 1$ and $(w^k)_{k \in \mathbb{N}}$ a random sequence generated by Algorithm 1 under Assumption 1 and step size condition (6). The following assertions hold:*

- i) *The sequence $(w^{k+1} - w^k)_{k \in \mathbb{N}}$ converges a.s. to zero.*
- ii) *The sequence $(\|w^k - \hat{w}\|)_{k \in \mathbb{N}}$ converges a.s. (not necessarily to zero) for every saddle point \hat{w} .*
- iii) *If every weak cluster point of $(w^k)_{k \in \mathbb{N}}$ is a.s. a saddle point, the sequence $(w^k)_{k \in \mathbb{N}}$ converges weakly a.s. to a saddle point.*

The key idea of the proof consists in rewriting Algorithm 1 as a sequence of operators $T_{\mathcal{S}}$ which depend on the random subsets \mathcal{S} . To show this, denote

$$w = (w_0, w_1, \dots, w_n) = (x, y_1, \dots, y_n)$$

and, for every $\mathcal{S} \subset \{1, \dots, n\}$, let the operator $T_{\mathcal{S}} : X \times Y \rightarrow X \times Y$ be defined by

$$(T_{\mathcal{S}}w)_i = \begin{cases} \text{prox}_{\tau g}(x - \tau A^*y - \sum_{j \in \mathcal{S}} (1 + p_j^{-1}) \tau A_j^*((T_{\mathcal{S}}w)_j - y_j)) & \text{if } i = 0 \\ \text{prox}_{\sigma_i f_i^*}(y_i + \sigma_i A_i x) & \text{if } i \in \mathcal{S} \\ y_i & \text{else} \end{cases}$$

Proposition 2. *Let $\theta = 1$ and $(w^k)_{k \in \mathbb{N}}$ a random sequence generated by Algorithm 1 under Assumption 1 and step size condition (6). The following assertions hold:*

i) *The iterates $(w^k)_{k \in \mathbb{N}}$ satisfy, for every $k \geq 0$,*

$$T_{\mathbb{S}^k}(x^{k+1}, y^k) = (x^{k+2}, y^{k+1}). \quad (11)$$

ii) *A point $w \in X \times Y$ is a saddle point if and only if it is a fixed point of $T_{\mathcal{S}}$ for every instance of \mathbb{S}^k .*

iii) *Every weak cluster point of $(w^k)_{k \in \mathbb{N}}$ is a.s. a saddle point.*

Proof of Theorem 1. By Proposition 2-iii), every weak cluster point of $(w^k)_{k \in \mathbb{N}}$ is almost surely a saddle point and, by Proposition 1-iii), the sequence $(w^k)_{k \in \mathbb{N}}$ converges weakly almost surely to a saddle point. \square

3.3. Proof of Propositions 1 & 2

We use the notation $\|x\|_T^2 = \langle Tx, x \rangle$ for any operator T . We also denote

$$V(x, y) := \|x\|_{\tau^{-1}}^2 + 2\langle QAx, y \rangle + \|y\|_{QS^{-1}}^2$$

with $S = \text{diag}(\sigma_1, \dots, \sigma_n)$ and A given by $(Ax)_i = A_i x$. For any $\hat{w} = (\hat{x}, \hat{y})$ we write

$$\Delta_{\hat{w}}^k := V(x^k - \hat{x}, y^{k-1} - \hat{y}) + \|y^k - \hat{y}\|_{QS^{-1}}^2$$

and the conditional expectation at time k is denoted as $\mathbb{E}^k(w) = \mathbb{E}(w \mid w^0, \dots, w^{k-1})$. With this notation we will make use of ([2], Lemma 4.1), which was originally obtained as a consequence of ([8], Lemma 4.4).

Lemma 2 ([2], Lemma 4.1). *Let $(w^k)_{k \in \mathbb{N}}$ be a random sequence generated by Algorithm 1 under Assumption 1. Then for every saddle point \hat{w} ,*

$$\Delta_{\hat{w}}^k \geq \mathbb{E}^{k+1}(\Delta_{\hat{w}}^{k+1}) + V(x^{k+1} - x^k, y^k - y^{k-1}). \quad (12)$$

In (12) we have simplified the original lemma by using the fact that Bregman distances of convex functionals are nonnegative [8]. We will also require the following lemma, which is equivalent to ([8], Lemma 4.2) with $\rho^2 = \max_i v_i/p_i$ and $c = \rho^{-1}$, and where we have replaced the ESO step size condition (9) with the equivalent condition (6).

Lemma 3 ([8], Lemma 4.2). *Let D be defined as in (5) such that $\|D\| = \rho^2$, and let $(y^k)_{k \in \mathbb{N}}$ be obtained through Algorithm 1. Then for all $x \in X$, $k \in \mathbb{N}$,*

$$\mathbb{E}^k V(x, y^k - y^{k-1}) \geq (1 - \rho) \mathbb{E}^k (\|x\|_{\tau^{-1}}^2 + \|y^k - y^{k-1}\|_{Q_{S^{-1}}}^2).$$

Proof of Proposition 1-i). Taking the expectation and applying Lemma 3 to (12) yields

$$\mathbb{E}(\Delta_{\hat{w}}^k) \geq \mathbb{E}(\Delta_{\hat{w}}^{k+1}) + (1 - \rho) \mathbb{E}(\|x^{k+1} - x^k\|_{\tau^{-1}}^2 + \|y^k - y^{k-1}\|_{Q_{S^{-1}}}^2).$$

Taking the sum from $k = 0$ to $k = N - 1$ gives

$$\Delta_{\hat{w}}^0 \geq \mathbb{E}(\Delta_{\hat{w}}^N) + (1 - \rho) \sum_{k=0}^{N-1} \mathbb{E} \left\{ \|x^{k+1} - x^k\|_{\tau^{-1}}^2 + \|y^k - y^{k-1}\|_{Q_{S^{-1}}}^2 \right\} \quad (13)$$

where we define $y^{-1} = y^0$. From Lemma 3 we know $\mathbb{E}(\Delta_{\hat{w}}^N) \geq 0$, hence taking the limit as $N \rightarrow \infty$ in (13) yields $\sum_{k=0}^{\infty} \mathbb{E}(\|x^{k+1} - x^k\|_{\tau^{-1}}^2 + \|y^k - y^{k-1}\|_{Q_{S^{-1}}}^2) < \infty$. By the monotone convergence theorem, this is equivalent to

$$\mathbb{E} \left\{ \sum_{k=0}^{\infty} \|x^{k+1} - x^k\|_{\tau^{-1}}^2 + \|y^k - y^{k-1}\|_{Q_{S^{-1}}}^2 \right\} < \infty, \quad (14)$$

which implies

$$\sum_{k=0}^{\infty} \|x^{k+1} - x^k\|_{\tau^{-1}}^2 + \|y^k - y^{k-1}\|_{Q_{S^{-1}}}^2 < \infty \quad \text{a.s.} \quad (15)$$

and it follows that a.s.

$$\|x^{k+1} - x^k\|_{\tau^{-1}} \rightarrow 0 \quad \text{and} \quad \|y^k - y^{k-1}\|_{Q_{S^{-1}}} \rightarrow 0. \quad (16)$$

Since these norms are equivalent to the usual norms in X and Y , we deduce the sequence $(w^{k+1} - w^k)_{k \in \mathbb{N}}$ converges to zero almost surely. \square

For the next part we require a slight variation of Lemma 3.

Lemma 4. *Let $\varphi = \max_i \|p_i^{-1/2} C_i\|$ and let $(y^k)_{k \in \mathbb{N}}$ be the iterates defined by Algorithm 1. For all $c > 0$, $x \in X$ and $k \in \mathbb{N}$, there holds*

$$V(x, y^k - y^{k-1}) \geq (1 - \frac{n\varphi}{c}) \|x\|_{\tau^{-1}}^2 + (1 - \varphi c) \|y^k - y^{k-1}\|_{Q_{S^{-1}}}^2.$$

Proof.

$$\begin{aligned} \langle QAx, y^k - y^{k-1} \rangle &= \sum_{i \in \mathbb{S}^k} \langle p_i^{-1} A_i x, y_i^k - y_i^{k-1} \rangle \\ &= \sum_{i \in \mathbb{S}^k} \langle p_i^{-1/2} C_i \tau^{-1/2} x, p_i^{-1/2} \sigma_i^{-1/2} (y_i^k - y_i^{k-1}) \rangle \\ &\leq \sum_{i \in \mathbb{S}^k} \|p_i^{-1/2} C_i\| \|x\|_{\tau^{-1}} \|y_i^k - y_i^{k-1}\|_{p_i^{-1} \sigma_i^{-1}} \\ &\leq \max_i \|p_i^{-1/2} C_i\| \sum_{i \in \mathbb{S}^k} \frac{1}{2} \left(\frac{1}{c} \|x\|_{\tau^{-1}}^2 + c \|y_i^k - y_i^{k-1}\|_{p_i^{-1} \sigma_i^{-1}}^2 \right) \\ &\leq \max_i \|p_i^{-1/2} C_i\| \frac{1}{2} \left(\frac{n}{c} \|x\|_{\tau^{-1}}^2 + c \|y^k - y^{k-1}\|_{Q_{S^{-1}}}^2 \right). \end{aligned}$$

□

We also recall a classical result by Robbins & Siegmund.

Lemma 5 ([32], Theorem 1). *Let \mathcal{F}_k be a sequence of sub- σ -algebras such that, for every k , $\mathcal{F}_k \subset \mathcal{F}_{k+1}$ and α_k, η_k are nonnegative \mathcal{F}_k -measurable random variables such that $\sum_{k=1}^{\infty} \eta_k < \infty$ a.s. and*

$$\mathbb{E}(\alpha_{k+1} | \mathcal{F}_k) \leq \alpha_k + \eta_k \quad \text{a.s.}$$

Then $(\alpha_k)_{k \in \mathbb{N}}$ converges almost surely to a random variable in $[0, \infty)$.

Proof of Proposition 1-ii). Let $c = (n+1)\varphi$. By Lemma 4, for any saddle point \hat{w}

$$\Delta_{\hat{w}}^k \geq \frac{1}{n+1} \|x^k - \hat{x}\|_{\tau^{-1}}^2 + (1 - (n+1)\varphi^2) \|y^k - y^{k-1}\|_{QS^{-1}}^2 + \|y^k - \hat{y}\|_{QS^{-1}}^2. \quad (17)$$

Since $y^k - y^{k-1} \rightarrow 0$ a.s. this implies $\Delta_{\hat{w}}^k$ is a.s. bounded from below, i.e. there exists a random variable $M_1 \geq 0$ (independent of k) such that $\alpha^k := \Delta_{\hat{w}}^k + M_1 \geq 0$ a.s. for every k . Let $\eta^k := 2|\langle QA(x^{k+1} - x^k), y^k - y^{k-1} \rangle|$. Then by (12),

$$\alpha^k + \eta^k \geq \mathbb{E}^{k+1}(\alpha^{k+1}) \quad \text{a.s. for every } k \quad (18)$$

where all terms are nonnegative and, for some $M_2 \geq 0$,

$$\begin{aligned} \eta^k &= 2|\langle QA(x^{k+1} - x^k), y^k - y^{k-1} \rangle| \leq 2\|QA\| \|x^{k+1} - x^k\| \|y^k - y^{k-1}\| \\ &\leq 2M_2 \|x^{k+1} - x^k\|_{\tau^{-1}} \|y^k - y^{k-1}\|_{QS^{-1}} \\ &\leq M_2 (\|x^{k+1} - x^k\|_{\tau^{-1}}^2 + \|y^k - y^{k-1}\|_{QS^{-1}}^2) \end{aligned}$$

which implies $\sum_{k=1}^{\infty} \eta^k < \infty$ a.s. by (15). Thus α^k satisfies Lemma 5 and we have

$$\Delta_{\hat{w}}^k \rightarrow \Delta_{\hat{w}} \quad \text{a.s. for some } \Delta_{\hat{w}} \in [-M_1, \infty).$$

Now since $(\Delta_{\hat{w}}^k)_{k \in \mathbb{N}}$ converges a.s. and is a.s. bounded, so is the right hand side of (17), and since $y^k - y^{k-1} \rightarrow 0$ a.s. we deduce that $(x^k, y^k)_{k \in \mathbb{N}}$ is a.s. bounded. Since x^k is a.s. bounded and $y^k - y^{k-1} \rightarrow 0$ a.s. it follows that

$$\langle QA(x^k - \hat{x}), y^k - y^{k-1} \rangle \rightarrow 0 \quad (19)$$

almost surely. From (16) and (19) we know some of the terms in

$$\Delta_{\hat{w}}^k = \|x^k - \hat{x}\|_{\tau^{-1}}^2 - 2\langle QA(x^k - \hat{x}), y^k - y^{k-1} \rangle + \|y^k - y^{k-1}\|_{QS^{-1}}^2 + \|y^k - \hat{y}\|_{QS^{-1}}^2$$

converge a.s. to zero, namely $\langle QA(x^k - \hat{x}), y^{k-1} - y^k \rangle$ and $\|y^{k-1} - y^k\|^2$, and thus the sequence $(\|x^k - \hat{x}\|_{\tau^{-1}}^2 + \|y^k - \hat{y}\|_{QS^{-1}}^2)_{k \in \mathbb{N}}$ converges a.s. to $\Delta_{\hat{w}}$. Finally, notice that the norm $\|w\|^2 := \|x\|_{\tau^{-1}}^2 + \|y\|_{QS^{-1}}^2$ is equivalent to the product norm $\|\cdot\|^2$ in $X \times Y$, hence since $(\|w^k - \hat{w}\|)_{k \in \mathbb{N}}$ converges a.s., so does $(\|w^k - \hat{w}\|)_{k \in \mathbb{N}}$. □

Proof of Proposition 1-iii). We follow closely the proof of ([12], Proposition 2.3). Let $(\Omega, \mathcal{F}, \mathbb{P})$ denote the probability space corresponding to the random sequence $(w^k)_{k \in \mathbb{N}}$, let \mathbf{F} be the set of solutions to (2) and let $\mathbf{G}(w^k)$ be the set of weak cluster points of the sequence $(w^k)_{k \in \mathbb{N}}$.

By Proposition 1-ii), the sequence $(\|w^k - w\|)_{k \in \mathbb{N}}$ converges a.s. for every solution $w \in \mathbf{F}$. Using ([12], Proposition 2.3-iii)), there exists $\Omega \in \mathcal{F}$ such that $\mathbb{P}(\Omega) = 1$ and the sequence $(\|w^k(\omega) - w\|)_{k \in \mathbb{N}}$ converges for every $w \in \mathbf{F}$ and $\omega \in \Omega$. This implies, since \mathbf{F} is nonempty, that $(w^k(\omega))_{k \in \mathbb{N}}$ is bounded and thus $\mathbf{G}(w^k(\omega))$ is nonempty for all $\omega \in \Omega$.

By assumption, there exists $\tilde{\Omega} \in \mathcal{F}$ such that $\mathbb{P}(\tilde{\Omega}) = 1$ and $\mathbf{G}(w^k(\omega)) \subset \mathbf{F}$ for every $\omega \in \tilde{\Omega}$. Let $\omega \in \Omega \cap \tilde{\Omega}$, then $(\|w^k(\omega) - w\|)_{k \in \mathbb{N}}$ converges for all $w \in \mathbf{G}(w^k(\omega)) \subset \mathbf{F}$. By ([12], Proposition 2.3-iv)), we have that $(w^k)_{k \in \mathbb{N}}$ converges weakly almost surely to an element of $\mathbf{G}(w^k) \subset \mathbf{F}$. \square

Proof of Proposition 2-i). By definition of the iterates in Algorithm 1, we have

$$(T_{\mathbb{S}^k}(x^{k+1}, y^k))_i = y_i^{k+1} \quad \text{for every } i \in \{1, \dots, n\}$$

and by induction it is easy to check that $z^k = A^*y^k$ for every $k \geq 0$, hence

$$\begin{aligned} \bar{z}^{k+1} &= z^{k+1} + \sum_{i \in \mathbb{S}^k} p_i^{-1} \delta_i = z^k + \sum_{i \in \mathbb{S}^k} (1 + p_i^{-1}) \delta_i = A^*y^k + \sum_{i \in \mathbb{S}^k} (1 + p_i^{-1}) A_i^*(y_i^{k+1} - y_i^k) \\ &= A^*y^k + \sum_{i \in \mathbb{S}^k} (1 + p_i^{-1}) A_i^*((T_{\mathbb{S}^k}(x^{k+1}, y^k))_i - y_i^k). \end{aligned}$$

Thus $(T_{\mathbb{S}^k}(x^{k+1}, y^k))_0 = \text{prox}_{\tau g}(x^{k+1} - \tau \bar{z}^{k+1}) = x^{k+2}$, which proves (11). \square

Proof of Proposition 2-ii). Let w be a fixed point of $T_{\mathcal{S}}$ for every instance of \mathbb{S}^k . By (4), for every $i \in \{1, \dots, n\}$ there exists an instance \mathcal{S} such that $i \in \mathcal{S}$ and

$$y_i = w_i = (T_{\mathcal{S}}w)_i = \text{prox}_{\sigma_i f_i^*}(y_i + \sigma_i A_i x).$$

Furthermore, for any \mathcal{S} ,

$$\begin{aligned} x = w_0 &= (T_{\mathcal{S}}w)_0 = \text{prox}_{\tau g}(x - \tau A^*y - \sum_{i \in \mathcal{S}} (1 + \frac{1}{p_i}) \tau A_i^*((T_{\mathcal{S}}w)_i - y_i)) \\ &= \text{prox}_{\tau g}(x - \tau A^*y). \end{aligned}$$

These conditions on x and y define a saddle point ([6], 6.4.2). The converse result is direct. \square

Proof of Proposition 2-iii). Let $v^k = (x^{k+1}, y^k)$ so that, by Proposition 2-i), we have $v^{k+1} = T_{\mathbb{S}^k}v^k$. From Proposition 1-i) we know

$$\|v^k - v^{k-1}\|^2 = \|x^{k+1} - x^k\|^2 + \|y^k - y^{k-1}\|^2 \rightarrow 0. \quad (20)$$

Taking the conditional expectation and denoting $p_{\mathcal{S}} := \mathbb{P}(\mathbb{S}^k = \mathcal{S})$ gives

$$\mathbb{E}^{k+1} \|v^{k+1} - v^k\|^2 = \mathbb{E}^{k+1} \|T_{\mathbb{S}^k}v^k - v^k\|^2 = \sum_{\mathcal{S}} p_{\mathcal{S}} \|T_{\mathcal{S}}v^k - v^k\|^2.$$

Thus by (20)

$$T_{\mathcal{S}}v^k - v^k \rightarrow 0 \quad \text{a.s.} \quad (21)$$

for every \mathcal{S} such that $p_{\mathcal{S}} > 0$. Now, let $w^{\ell_k} \rightharpoonup w^*$ be a weakly convergent subsequence. From (20) we know $y^k - y^{k-1} \rightarrow 0$ a.s. and so v^{ℓ_k} also converges weakly to w^* . This, together with (21) implies, for all $u \in X \times Y$ and all \mathcal{S} such that $p_{\mathcal{S}} > 0$,

$$\langle w^*, u \rangle = \lim_{k \rightarrow \infty} \langle v^{\ell_k}, u \rangle = \lim_{k \rightarrow \infty} \langle T_{\mathcal{S}}v^{\ell_k}, u \rangle \quad \text{a.s.}$$

and, by the weak sequential continuity of $T_{\mathcal{S}}$ (Assumption 1), it follows that

$$\lim_{k \rightarrow \infty} \langle T_{\mathcal{S}}v^{\ell_k}, u \rangle = \langle T_{\mathcal{S}}(\lim_{k \rightarrow \infty} v^{\ell_k}), u \rangle = \langle T_{\mathcal{S}}w^*, u \rangle$$

almost surely. Hence w^* is almost surely a fixed point of $T_{\mathcal{S}}$ for each instance of \mathbb{S}^k . By Proposition 2-ii), w^* is a saddle point. \square

4. Step size parameters

Theorem 1 requires a choice of step size parameters τ, σ_i that satisfy condition (6), i.e. $\|D\| < 1$. In this section we illustrate how to choose adequate step sizes for specific examples of random samplings, starting with the general case of not necessarily strongly convex functions. Furthermore, if the functionals g, f_i^* are strongly convex, then optimal step sizes can be determined that offer linear convergence rate [8].

4.1. The general convex case

4.1.1. Serial sampling For serial sampling, a valid step size choice is given by

$$\tau \sigma_i \|A_i\|^2 < p_i \quad \text{for every } i \in \{1, \dots, n\}. \quad (22)$$

Indeed this implies (6) since, for serial sampling, (22) gives

$$\|Dz\| = \mathbb{E} \|C_{\mathbb{S}}^* Qz\|^2 = \sum_{i=1}^n p_i \|C_i^* p_i^{-1} z\|^2 = \sum_{i=1}^n p_i^{-1} \tau \sigma_i \|A_i^* z\|^2 < \|z\|^2.$$

This insight can be generalized as follows.

4.1.2. b-serial sampling Consider a partition of the set $\{1, \dots, n\}$ into m blocks I_j , i.e.

$$\bigcup_{j=1}^m I_j = \{1, \dots, n\} \quad \text{and} \quad I_j \cap I_l = \emptyset \quad \text{for all } j \neq l.$$

At every iteration we select a single block $j \in \{1, \dots, m\}$ and update every index $i \in I_j$. For such a sampling, step size condition (22) reads

$$\tau \sigma_i \|\tilde{A}_j\|^2 < \tilde{p}_j \quad \text{for } i \in I_j, j \in \{1, \dots, m\} \quad (23)$$

where \tilde{p}_j is the probability of choosing block I_j and $\tilde{A}_j : X \rightarrow \prod_{i \in I_j} Y_i$ is the operator

$$\tilde{A}_j x = (A_i x)_{i \in I_j}.$$

Notice we assumed every index i within a block I_j to have the same dual step size σ_i . We refer to this random process as *b-serial sampling* when all subsets have size b , i.e. $|I_j| = b$ for all $j \in \{1, \dots, m\}$, with $1 \leq b \leq n$.

In general, this form of sampling is equivalent to serial sampling where the operators \tilde{A}_j have taken the role of the A_i , however, we make this distinction to focus on parameter b , the batch size, which will be an important variable for our numerical experiments. We will still refer to it as serial sampling when referring to the case $b = 1$.

4.1.3. b-nice sampling Consider now the random sampling \mathbb{S} that randomly selects b elements from $\{1, \dots, n\}$ at each iteration, i.e. every instance of \mathbb{S} is a random subset of size b . Clearly at each iteration there are $\binom{n}{b}$ possible choices. This process is different from *b-serial sampling*, since the subsets are not disjoint and do not form a partition of $\{1, \dots, n\}$.

In this paper we will assume uniform *b-nice sampling*, i.e. all possible instances of \mathbb{S} have equal probability. In this case, it is easy to see the probabilities $p_i = \mathbb{P}(i \in \mathbb{S})$ are given by $p_i = b/n$, and condition (10) reads

$$\frac{\tau \sigma n^2}{b^2} \|\mathbb{E}(A_{\mathbb{S}} A_{\mathbb{S}}^*)\| < 1. \quad (24)$$

4.2. The strongly convex case

Algorithm 1 has linear convergence for strongly convex functionals g, f_i^* [8]. Here, we have replaced the ESO parameter condition $v_i < \theta^{-1} p_i$ from the original theorem with the equivalent condition $\|D\| < \theta^{-1}$, as explained in Lemma 1.

Lemma 6 ([8], Theorem 6.1). *Let g, f_i^* be strongly convex with parameters $\mu_g, \mu_i > 0$ for $i \in \{1, \dots, n\}$ and let (\hat{x}, \hat{y}) be the unique solution of (2). Let D satisfy*

$$\|D\| < \frac{1}{\theta} \quad (25)$$

where the extrapolation $\theta \in (0, 1)$ satisfies the lower bounds

$$\theta \geq \frac{1}{1 + 2\mu_g \tau}, \quad \theta \geq \max_i 1 - 2 \frac{\mu_i \sigma_i p_i}{1 + 2\mu_i \sigma_i}. \quad (26)$$

Then Algorithm 1 converges with rate $\mathcal{O}(\theta^k)$.

Furthermore, it is possible to estimate the optimal (smallest) value of θ by equating the lower bounds in (26) together with step size condition (25) [8]. For instance, from (10) we know that, for uniform step sizes, condition (25) is satisfied by

$$\tau \sigma \|B\| \theta = \rho^2$$

where $B = Q(\mathbb{E}(A_{\mathbb{S}} A_{\mathbb{S}}^*)Q$ and $\rho \in (0, 1)$. This together with (26) yields

$$\theta = \max_i 1 - \frac{2p_i}{1 + \sqrt{\beta_i}} \quad (27)$$

where $\beta_i = 1 + \|B\| p_i / (\mu_g \mu_i \rho^2)$, and the corresponding optimal step sizes are

$$\tau = \min_i \frac{\mu_g^{-1} p_i}{1 - 2p_i + \sqrt{\beta_i}}, \quad \sigma = \min_i \frac{\mu_i^{-1}}{\sqrt{\beta_i} - 1}. \quad (28)$$

4.2.1. Serial sampling Better theoretical convergence rates can be computed if more is known about the sampling. In particular, optimal convergence rates for uniform and non-uniform serial sampling have been proposed in [8]. These are, for uniform serial sampling,

$$\theta_{us} = 1 - \frac{2}{n + n \max_i \sqrt{\alpha_i}}$$

where $\alpha_i = 1 + \|A_i\|^2 / (\mu_g \mu_i \rho^2)$, $p_i = b/n$ and step size parameters given by

$$\tau = \frac{\mu_g^{-1}}{n - 2 + n \max_j \sqrt{\alpha_j}}, \quad \sigma_i = \frac{\mu_i^{-1}}{\max_j \sqrt{\alpha_j} - 1}, \quad i \in \{1, \dots, n\}. \quad (29)$$

and for serial sampling with optimized probabilities,

$$\theta_{os} = 1 - \frac{2}{n + \sum_{i=1}^n \sqrt{\alpha_i}}$$

where the optimal probabilities are found to be

$$p_i = \frac{1 + \sqrt{\alpha_i}}{n + \sum_{j=1}^n \sqrt{\alpha_j}}, \quad i \in \{1, \dots, n\} \quad (30)$$

and the step size parameters are

$$\tau = \frac{\mu_g^{-1}}{n - 2 + \sum_{j=1}^n \sqrt{\alpha_j}}, \quad \sigma_i = \frac{\mu_i^{-1}}{\sqrt{\alpha_i} - 1}, \quad i \in \{1, \dots, n\}. \quad (31)$$

In general $\theta_{os} \leq \theta_{us}$, as the former imposes less restrictions over probabilities p_i .

4.2.2. b-serial sampling These last results are also useful for b -serial sampling. To see this we define \tilde{A}_j and \tilde{p}_j as in (23) and \tilde{f}_j^* as

$$\tilde{f}_j^*(\tilde{y}_j) = \sum_{i \in I_j} f_i(y_i), \quad \tilde{y}_j \in \prod_{i \in I_j} Y_i, \quad j \in \{1, \dots, m\}.$$

With this notation, our original (strongly convex) saddle point problem (2) becomes

$$\hat{x}, \hat{y} \in \arg \min_{x \in X} \max_{\tilde{y} \in Y} \sum_{j=1}^m \langle \tilde{A}_j x, \tilde{y}_j \rangle - \tilde{f}_j^*(\tilde{y}_j) + g(x)$$

where $\tilde{y} = (\tilde{y}_1, \dots, \tilde{y}_m)$ and \tilde{f}_j^* are strongly convex with parameters $\tilde{\mu}_j = \min\{\mu_i \mid i \in I_j\}$. Thus Lemma 6 guarantees the linear convergence of Algorithm 1 and, as before, the optimal convergence rates are

$$\theta_{us} = 1 - \frac{2}{m + m \max_j \sqrt{\tilde{\alpha}_j}}, \quad \theta_{os} = 1 - \frac{2}{m + \sum_{j=1}^m \sqrt{\tilde{\alpha}_j}} \quad (32)$$

with $\tilde{\alpha}_j = 1 + \|\tilde{A}_j\|^2 / (\mu_g \tilde{\mu}_j \rho^2)$. In both cases, the optimal step size parameters $\tau, \tilde{\sigma}_j$ are also given as in (29) or (31). The optimal probabilities are given by (30).

Notice how the optimal convergence rates θ_{us} and θ_{os} depend on b . In particular, choosing $b = n$ gives us the optimal step sizes for the PDHG algorithm (2), i.e. SPDHG with full sampling. In this case, $m = 1$ and the optimal convergence rate is

$$\theta_{us} = \theta_{os} = 1 - \frac{2}{1 + \sqrt{1 + \frac{\|A\|^2}{\mu_g \mu_{f^*} \rho^2}}} \quad (33)$$

where $\mu_{f^*} = \min\{\mu_1, \dots, \mu_n\}$ is the convexity parameter of $f^*(y) = \sum_{i=1}^n f_i^*(y_i)$.

Notice as well that there is more than one way to partition the set $\{1, \dots, n\}$ into m subsets I_j of size b . For instance, if n is divisible by b , the number \mathbf{k} of different partitions of $\{1, \dots, n\}$ into subsets of size b is

$$\mathbf{k}(n, b) = \prod_{j=1}^{\frac{n}{b}} \binom{jb-1}{b-1}. \quad (34)$$

Moreover, the optimal convergence rates θ_{us} and θ_{os} will also depend on which partition we use, since the subsets I_j define in turn the values $\tilde{\mu}_j$ and $\|\tilde{A}_j\|$. In Section 5, we will see examples of how using a different partition of $\{1, \dots, n\}$ can improve the convergence rate of SPDHG with b -serial sampling.

4.2.3. b-nice sampling For uniform b -nice sampling we use rate (27) with uniform probability $p_i = b/n$, and we denote

$$\theta_{un} = 1 - \frac{2b}{n + n \max_i \sqrt{\beta_i}} \quad (35)$$

with step size parameters given as in (28).

This quantity also depends strongly on the batch size b since the probabilities p_i and thus also the norm of the operator B are determined by b . In particular, choosing $b = n$ in (35) results in $p_i = 1$ and $\|B\| = \|AA^*\| = \|A\|^2$, hence we recover the same full sampling convergence rate (33) from b -serial sampling.

5. Parallel MRI reconstruction

In this section we take real MRI data and perform parallel MRI reconstruction with sensitivity encoding using SPDHG [17, 30]. For more examples on stochastic methods applied to MRI reconstruction, see [25]. For our experiments, the data have been sourced from the NYU fastMRI dataset [22, 38].

For a system with n coils, we are given n data b_1, \dots, b_n which relate to the inverse problems $b_i = A_i x + \eta_i$, where each $A_i : \mathbb{C}^{d_1} \rightarrow \mathbb{C}^{d_2}$ is the forward operator from the signal space to the sample space, and $\eta_i \in \mathbb{C}^{d_2}$ represents random noise. The data are undersampled, i.e. $A_i = S \circ F \circ C_i$, where $S : \mathbb{C}^{d_1} \rightarrow \mathbb{C}^{d_2}$ is a subsampling operator, $F : \mathbb{C}^{d_1} \rightarrow \mathbb{C}^{d_1}$ represents the discrete Fourier transform and $C_i x = c_i \cdot x$ is the element-wise multiplication of x and the i -th coil-sensitivity map $c_i \in \mathbb{C}^{d_1}$. Figure 1a shows the magnitude of the coil sensitivity maps c_i , obtained using sigpy's *EspiritCalib* method [24] on a dataset collected using $n = 12$ coils, arranged uniformly in a circle around a patient's head.

An image \hat{x} is then reconstructed from the data by solving the regularized least-squares problem

$$\hat{x} \in \arg \min_x \sum_{i=1}^n \frac{1}{2} \|A_i x - b_i\|^2 + g(x) \quad (36)$$

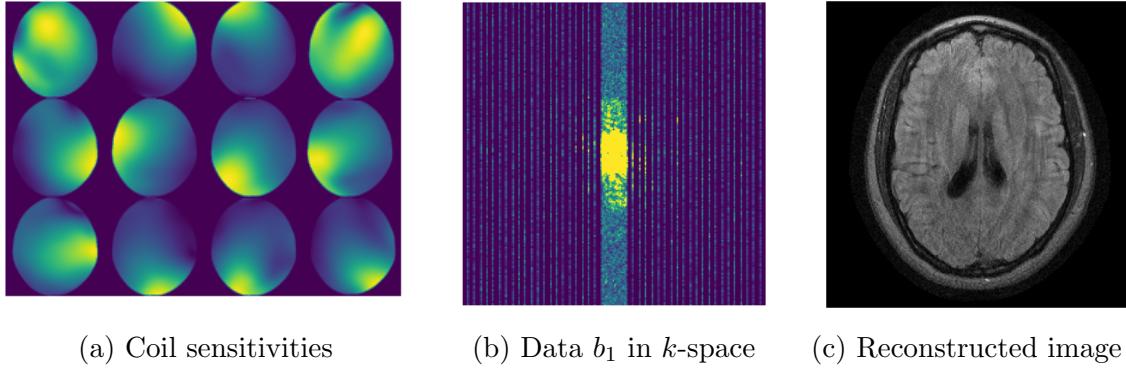


Figure 1: **Parallel MRI reconstruction with $n = 12$ coils.** (a) Spatial visualization of coil sensitivities for an MRI scanner with 12 electromagnetic coils distributed uniformly in a circle. (b) Data collected by a single coil, encoded in Fourier space. (c) A reconstructed image obtained using sigpy's SenseRecon method [24].

where g is a regularizer. We recover our convex minimization template (1) by identifying \mathbb{C}^d with \mathbb{R}^{2d} and setting $X = \mathbb{R}^{2d_1}$, $Y_i = \mathbb{R}^{2d_2}$ and $f_i(y) = \|y - b_i\|^2$.

In order to test performance of SPDHG we look into the convergence of its iterations (x^k, y^k) at every epoch. We consider an epoch as the number of iterations required to perform the same amount of computational work (e.g. linear operations) as one iteration of the deterministic PDHG method. In particular, for b -serial and b -nice samplings, where one epoch is roughly equivalent to $m = n/b$ iterations, we define the *relative primal error* as

$$\mathbf{e}_b(k) := \frac{\|x^{mk} - \hat{x}\|}{\|\hat{x}\|},$$

where \hat{x} is a (fixed) solution of (36). In our experiments, \hat{x} is obtained using sigpy's SenseRecon [24] or the deterministic PDHG method [12] for 10^4 iterations.

Similarly, the convergence rate θ from Lemma 6 holds at every iteration k , hence for b -serial and b -nice sampling we can define the *convergence rates per epoch* as

$$\vartheta_{us} = (\theta_{us})^m, \quad \vartheta_{os} = (\theta_{os})^m, \quad \vartheta_{un} = (\theta_{un})^m$$

with θ_{us} , θ_{os} and θ_{un} defined as in (32) and (35).

All our experiments are implemented in Python using the Operator Discretization Library (ODL) [1]. The code for SPDHG's algorithm is based on the original implementation from [8]. Operator norms such as $\|B\|$ are computed using the power method in ODL.

5.1. L^2 regularization

Consider model (36) with L^2 regularizer $g = \frac{\lambda}{2} \|\cdot\|^2$. In this setting, functionals f_i^* , g are strongly convex with convexity parameters $\mu_i = 1$ for all i and $\mu_g = \lambda$, respectively. Hence for both b -serial and b -nice samplings, we can use Lemma 6 to determine the optimal step size parameters τ, σ_i and the optimal rate of convergence θ .

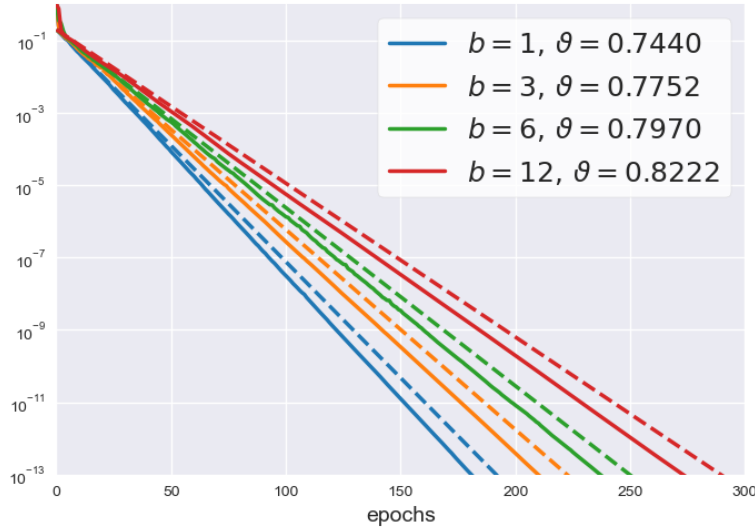
(a) \mathbf{e}_b for optimal b -serial sampling

Figure 2: **Convergence of SPDHG for MRI- L^2 .** Relative primal error \mathbf{e}_b for optimized b -serial sampling with different values of batch size b . The observed performance matches the theoretical convergence rate per epoch ϑ_{os} , shown as a dashed line for each b . The convergence rate per epoch ϑ_{os} improves for smaller batch sizes.

Figure 2 shows the performance of solving (36) with L^2 regularizer and $\lambda = 10^{-2}$ using SPDHG with optimal b -serial sampling. For each b it shows the relative primal error \mathbf{e}_b along with its optimal convergence rate per epoch ϑ_{os} . Each curve is the average of 10 independent runs. We see that the theoretical convergence rate is a good indicator of the actual performance of the algorithm.

When considering b -serial sampling, it is necessary to partition the data into n/b subsets of size b . The most natural partition of $\{1, \dots, n\}$ is perhaps the *consecutive* partition, which consists of the subsets $I_j = \{(j-1)b, (j-1)b+1, \dots, jb\}$ so that

$$\{1, \dots, n\} = \bigcup_{j=1}^m I_j = \{1, \dots, b\} \cup \{b+1, \dots, 2b\} \cup \dots \cup \{n-b+1, \dots, n\}. \quad (37)$$

However, as stated in Section 4, this is not the only way to partition $\{1, \dots, n\}$ into m subsets of size b . For instance, from (34) we know the number of partitions for $n = 12$ and $b = 6$ is $\binom{11}{5} = 462$, while for $b = 2$ the number is $\binom{3}{1} \binom{5}{1} \binom{7}{1} \binom{9}{1} \binom{11}{1} = 10\,395$. For each one of these partitions it is possible to compute the optimal convergence rates per epoch ϑ_{os} and ϑ_{us} .

Figures 3a and 3b show the distribution of these rates over all possible partitions for $n = 12$ and $b = 4$, for optimal and uniform b -serial sampling, respectively. The value of the theoretical convergence rate for b -nice sampling (ϑ_{un}) is shown in blue. In Figure 3b we see that uniform b -nice sampling has a better (lower) convergence rate than uniform b -serial sampling with most possible partitions. In Figure 3a, uniform b -nice performs better than the worst partition for optimal b -serial, but worse than the

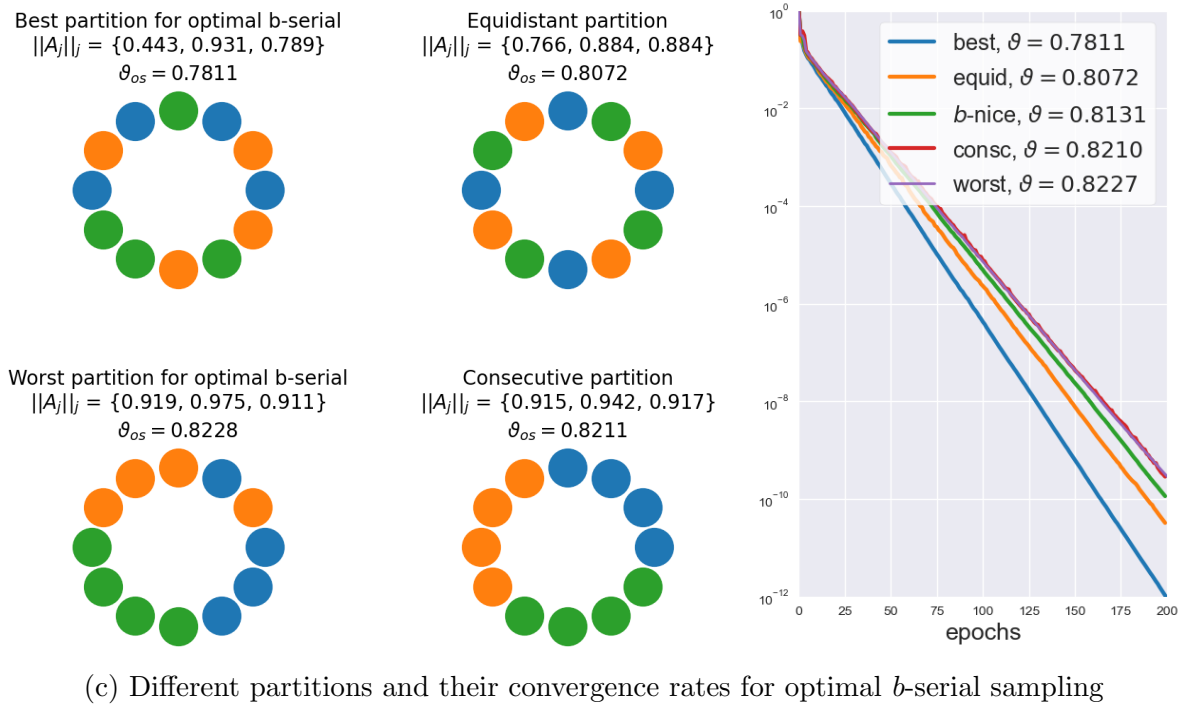
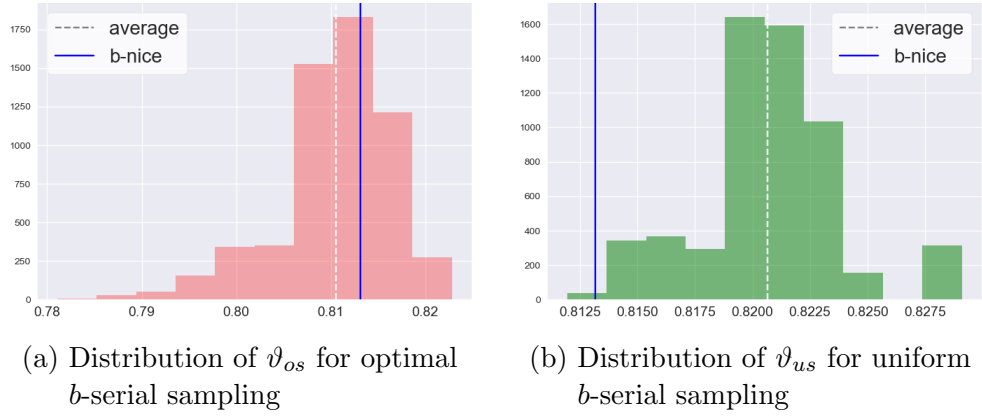


Figure 3: **Convergence rate for all partitions of batch size $b = 4$.** Figures (a) and (b) show the distribution of convergence rates per epoch for optimal b -serial sampling (ϑ_{os}) and for uniform b -serial sampling (ϑ_{us}) for all possible 5775 partitions (34). The convergence rate per epoch for uniform b -nice sampling is shown in blue (ϑ_{un}). Figure (c) show the subsets of coils that conform the best and worst partition from the histogram in (a), as well as two other partitions of interest. Figure (d) shows the relative primal error \mathbf{e}_b for each of the partitions shown in (c), as well as the performance of uniform b -nice sampling. Performance is significantly improved by choosing the right partition.

average partition.

From the values that conform Figure 3a, we have identified the partitions that

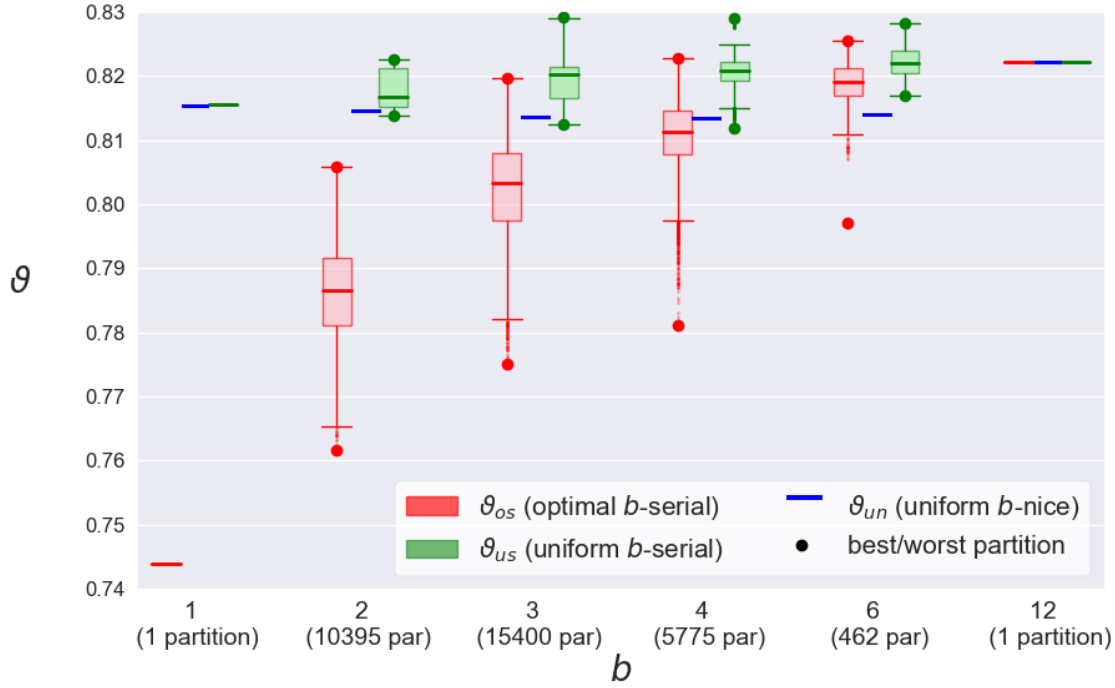


Figure 4: **Distribution of optimal convergence rate ϑ .** Optimal theoretical rates per epoch for optimal b -serial sampling (ϑ_{os}) and uniform b -serial sampling (ϑ_{us}) for all possible partitions of batch size b , for each b . The rate for the best and worst partition is highlighted in each case. Uniform b -nice sampling performs better than uniform b -serial sampling for most partitions, except for the best partition. In all cases, optimal b -serial sampling outperforms the other two samplings when using its best partition.

correspond to the best and worst convergence rate ϑ_{os} . These two partitions are

$$\begin{aligned} \mathbf{P}_{os}^{best} &= \left\{ \{1, 3, 5, 7\}, \{2, 6, 10, 12\}, \{4, 8, 9, 11\} \right\}, \\ \mathbf{P}_{os}^{worst} &= \left\{ \{1, 3, 11, 12\}, \{2, 4, 5, 6\}, \{7, 8, 9, 10\} \right\}. \end{aligned} \quad (38)$$

The corresponding coils and their positions are shown in Figure 3c and their corresponding ϑ_{os} values are $\vartheta_{os}^{best} = 0.7811$ and $\vartheta_{os}^{worst} = 0.8228$. The performance of Algorithm 1 with optimal b -serial sampling using these two partitions is also illustrated in Figure 3c. Notice how there is a significant improvement in performance by choosing the correct partition. Furthermore, the error \mathbf{e}_b for optimal b -serial sampling with the consecutive partition is almost as bad as using the worst possible partition.

Figure 3c also suggest that the physical locations of the coils may determine the best and worst partitions. This supports the intuitive notion that, since coils that are closer together correspond to more correlated forward operators A_i , the best partition may be the one that maximizes correlation between its subsets and minimizes correlation within each subset, i.e. minimizes the value of the operator norms $\|\tilde{A}_j\|$. Furthermore, from definition (32) we expect the optimal partition for optimal b -serial sampling to be such that $\sum_j \|\tilde{A}_j\|$ is minimized, while for uniform b -serial sampling the optimal partition

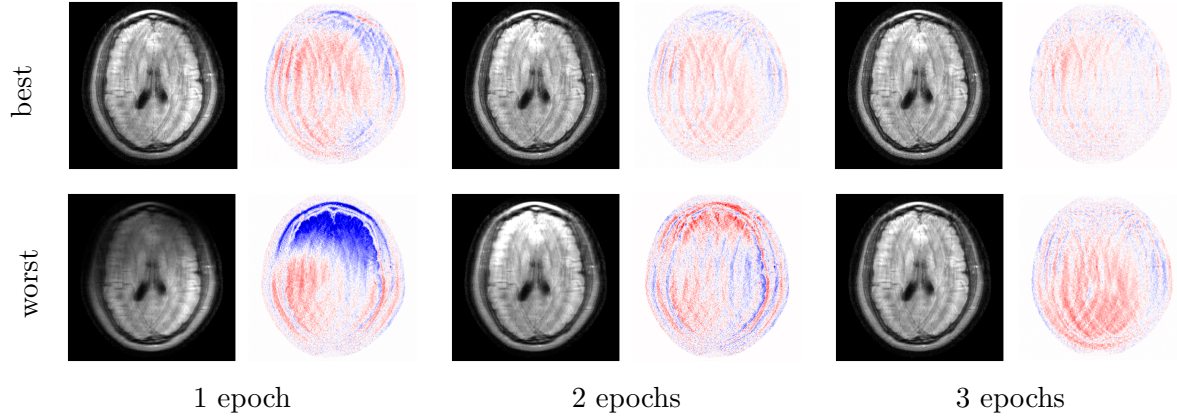


Figure 5: **MRI reconstruction with the best and worst possible sampling.** Reconstructed image $|x^k|$ and real error $\text{Re}(x^k - \hat{x})$, obtained using SPDHG with the best possible sampling, i.e. optimal serial sampling on $b = 1$ (top) and with the worst possible sampling, i.e. uniform b -serial sampling with $b = 3$ on the worst partition (bottom). The performance of SPDHG seems to correspond to the theoretical convergence rates, as suggested in Figure 4.

should minimize $\max_j \|\tilde{A}_j\|$.

With this intuition we test two other partitions of interest: the *consecutive* partition and the *equidistant* partition, also shown in Figure 3c. For the reasons mentioned above, we expect the consecutive partition to perform poorly, and the equidistant partition to be among the better choices of partitions. However, our numerical experiments show that in general this is not so straightforward, and that the best and worst partitions are determined by more than just the spatial location of the receiving coils.

The histograms in Figure 3 can also be computed for all other values of b in order to find their best and worst partitions. In fact, the experiments shown in Figure 2 use the best partitions \mathbf{P}_{os}^{best} and \mathbf{P}_{us}^{best} for optimized and uniform b -serial samplings respectively, for each batch size b .

Figure 4 shows the distributions of ϑ_{os} and ϑ_{us} for all possible partitions and all possible values of b . Trivially, for the special cases of $b = 1$ and $b = n$ there is only one possible partition. The rate ϑ_{un} for uniform b -nice sampling is independent of any partition. Notice how for serial sampling ($b = 1$) the values ϑ_{us} and ϑ_{un} are very similar, while optimal serial sampling offers significant improvement. For $b = n$, all three samplings are identical as they all imply the fully deterministic PDHG, thus $\vartheta_{os} = \vartheta_{us} = \vartheta_{un}$.

In general, for most values of b uniform b -nice sampling performs better than uniform b -serial for most partitions. For larger values of b , uniform b -nice also seems to perform better than the average partition for optimal b -serial. In particular for $b = 6$ b -nice sampling performs better than the average partition of optimal b -serial sampling and better than any partition of uniform b -serial sampling. In all cases, optimal b -serial sampling yields significantly better convergence rates than the other uniform b -serial

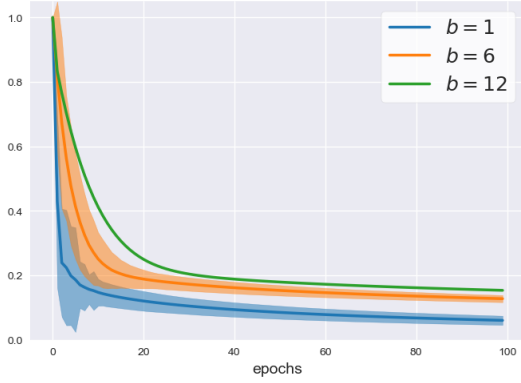
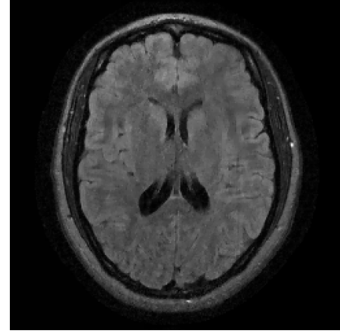
(a) Mean error $\mathbf{e}_b \pm$ its standard deviation(b) Solution \hat{x}

Figure 6: **SPDHG for MRI-TV with uniform b -serial sampling.** Average relative primal error \mathbf{e}_b plus/minus its standard deviation, out of 10 independent runs. Variation goes to zero as the algorithm converges to a solution. The special case $b = n$ is deterministic and has no variance. The target solution \hat{x} was obtained after 10^4 iterations of PDHG.

samplings when using its best possible partition.

Using the results from Figure 4 we can identify the best and worst possible samplings for SPDHG. The sampling with lowest convergence rate ϑ is attained at $b = 1$ with optimal serial sampling, while the worst rate is given by $b = 3$ with uniform serial sampling with the worst partition. Figure 5 shows the result of using these two different samplings on the same reconstruction problem. One sees that the convergence rates have a clear effect on the efficiency of SPDHG, and that the performance of SPDHG can in general be determined by the choice of sampling.

5.2. Total Variation regularization

Consider now the *total variation* (TV) regularizer $g = \lambda \|\nabla \cdot\|_1$ [33]. In our experiments, its proximity operator $\text{prox}_{\tau g}$ is approximated iteratively using the Fast Iterative Shrinkage/Thresholding Algorithm (FISTA) with warm starting [4]. Unless stated otherwise, in most of our experiments the number of iterations of FISTA per epoch of SPDHG is the same, so different samplings can be compared.

For b -serial sampling, we satisfy step-size condition (23) by choosing

$$\tau = \frac{\rho}{\gamma} \quad \sigma_i = \frac{\rho \gamma \tilde{P}_j}{\|\tilde{A}_j\|^2}, \quad i \in I_j \quad j \in \{1, \dots, m\} \quad (39)$$

where $\rho \in (0, 1)$ and $\gamma > 0$.

Figure 6a shows the performance of SPDHG applied to (36) with $\lambda = 10^2$, using uniform b -serial sampling and step sizes chosen as in (39) with $\rho = 0.98$ and $\gamma = 1$. At every iteration, the approximation of the proximal operator $\text{prox}_{\tau g}$ is updated using $12/m = 12b/n$ FISTA iterations, so that there are 12 FISTA iterations per epoch in

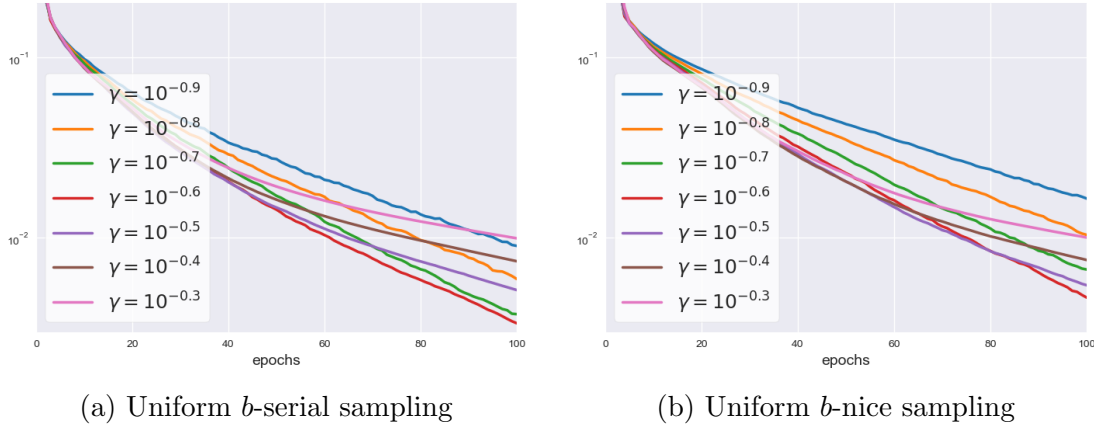


Figure 7: **SPDHG with different step size parameters.** Relative primal error \mathbf{e}_b for $b = 1$ and different values of step size parameters τ and σ_i , determined by γ as in (39) for b -serial sampling and as in (40) for b -nice sampling (b). While for each i the product $\sigma_i\tau$ is constant over γ , the effect of γ is visible for every choice.

Table 1: **Optimal γ for each b (at 100 epochs).**

	$b = 1$	$b = 2$	$b = 3$	$b = 4$	$b = 6$	$b = 12$
uniform b -serial	$10^{-0.6}$	$10^{-0.9}$	$10^{-1.1}$	$10^{-1.2}$	$10^{-1.3}$	$10^{-1.6}$
uniform b -nice	$10^{-0.6}$	$10^{-0.9}$	$10^{-1.0}$	$10^{-1.2}$	$10^{-1.3}$	$10^{-1.6}$

any given sampling. The solid lines represent the mean μ of the relative primal error \mathbf{e}_b for 10 different runs of the algorithm, while the shaded color represents the area between $\mu(\mathbf{e}_b) + \sigma(\mathbf{e}_b)$ and $\mu(\mathbf{e}_b) - \sigma(\mathbf{e}_b)$, where $\sigma(\mathbf{e}_b)$ is the standard deviation. The error \mathbf{e}_b in Figure 6a is computed using a solution \hat{x} obtained after 10^4 iterations of the deterministic PDHG algorithm, shown in Figure 6b. Notice how the variance of the iterations decreases over time. In addition, using smaller batch size b shows faster convergence and larger variance at the same time. Trivially, when $b = n$ this is simply the deterministic PDHG method (3) and it has no variance.

In contrast with the L^2 regularization model, the TV regularizer g is not strongly convex and Lemma 6 does not apply. Hence for this model we do not have a formula for determining the optimal step sizes. Instead, for each sampling we test performance for different values of τ, σ_i , chosen as in (39) and (40) with $\rho = 0.98$ and

$$\gamma \in \{10^{-2}, 10^{-1.9}, 10^{-1.8}, \dots, 10^{1.8}, 10^{1.9}, 10^2\}.$$

Here, γ represents the trade-off between the primal and the dual step sizes. Figure 7a shows the performance of SPDHG with uniform serial sampling for some values of γ . The choice of step size parameters has an effect in performance even if for all these choices the step size condition (22) is satisfied in exactly the same way, i.e. $\tau\sigma_i\|A_i\|^2 = \rho p_i$ for all values of γ .

In this way we can determine a good choice of γ by trying different values and

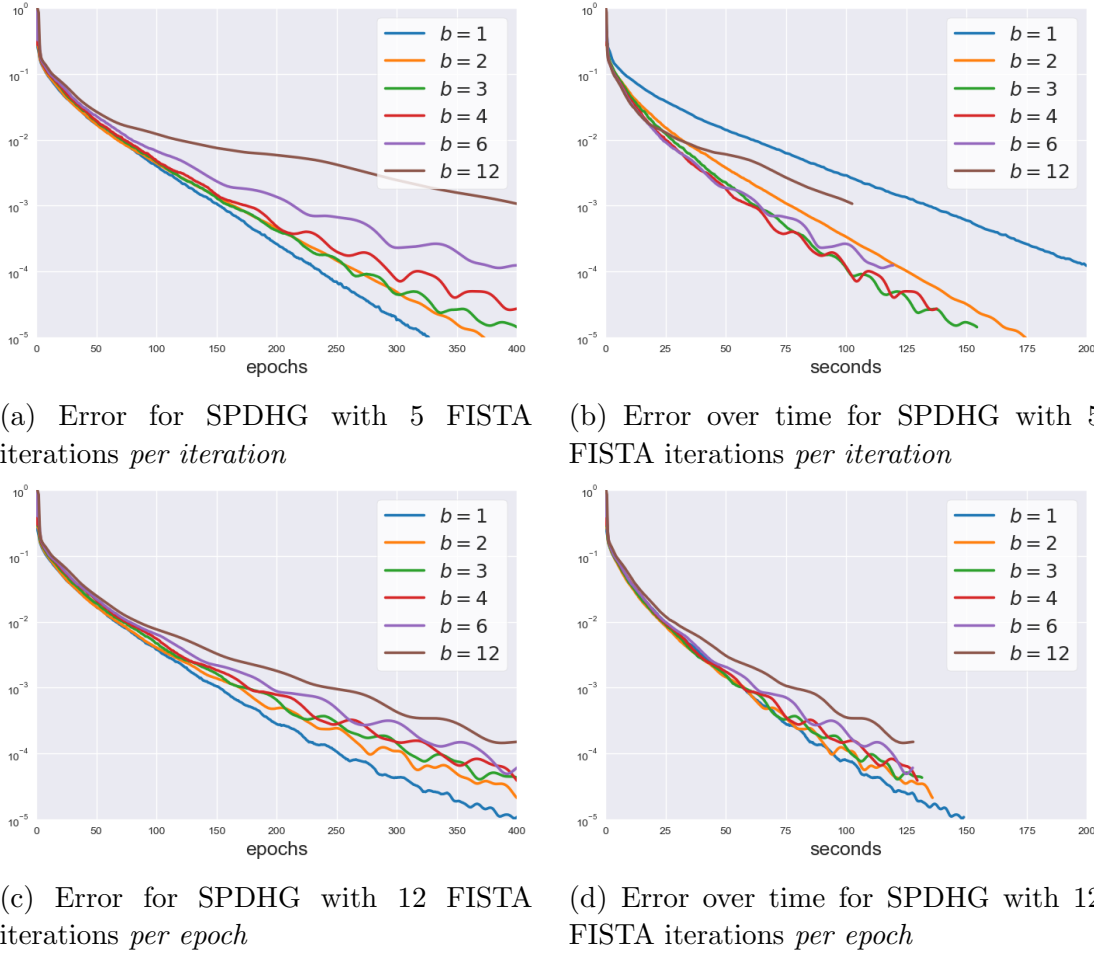


Figure 8: **Performance of SPDHG with uniform b -serial sampling.** Relative primal error \mathbf{e}_b for SPDHG with uniform b -serial sampling, with step size parameters determined by the optimal γ from Table 1, for each b . The error is plotted over epochs (left) and over computational time (right). Both the accuracy and the computational workload of the algorithm are drastically different when the number of FISTA iterations is chosen to be fixed per iteration or per epoch of SPDHG.

selecting the one that results in the smallest error $\mathbf{e}_b(k)$ at a fixed epoch $k = 100$. Doing this for each b we find an “optimal” γ denoted γ_b . The results are listed in Table 1. The same experiment is performed in Figure 7b for uniform b -nice sampling, where the step size condition (24) is satisfied by

$$\tau = \frac{\rho}{\gamma} \quad \sigma_i = \frac{\rho\gamma b^2}{n^2 \|\mathbb{E}(A_{\mathbb{S}} A_{\mathbb{S}}^*)\|^2} \quad i \in \{1, \dots, n\}, \quad (40)$$

and the optimal values of γ are also registered in Table 1. One notices from Table 1 that the optimal γ depends on b but is more or less consistent across the two samplings.

Having established a suitable γ_b for each b , Figure 8 shows the performance of uniform b -serial sampling using the corresponding optimal values γ_b . Figures 8a and 8c show the accuracy of SPDHG with b -serial sampling for 100 epochs. As in the strongly

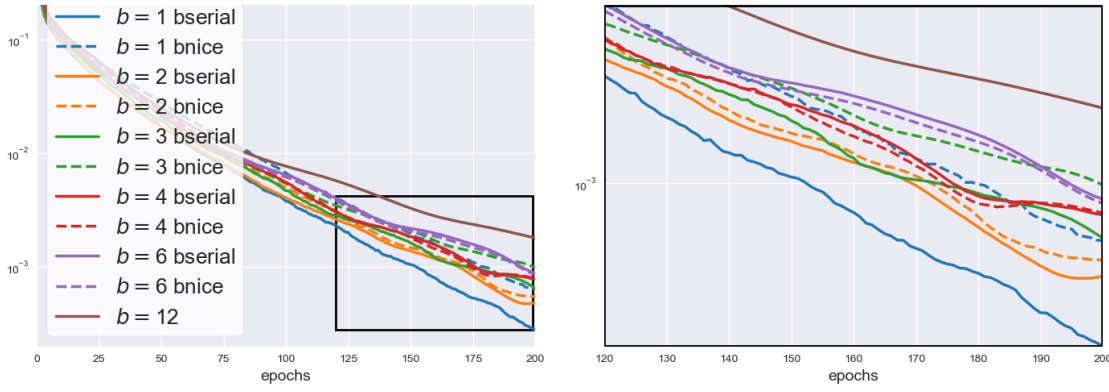


Figure 9: **Uniform b -serial sampling versus uniform b -nice sampling.** Relative primal error e_b for SPDHG with uniform b -serial (solid) and uniform b -nice sampling (dashed). For b -serial, smaller batch size seems to yield better performance, while for b -nice the difference between batches is less clear.

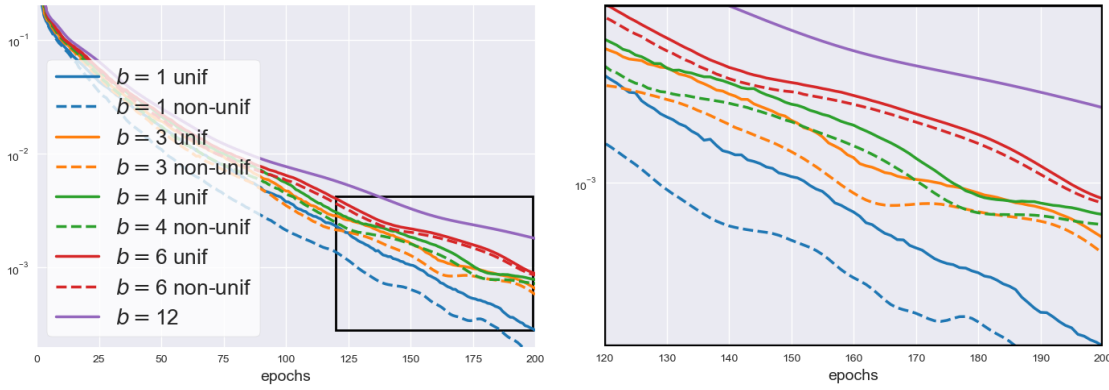


Figure 10: **Uniform versus non-uniform b -serial sampling.** Relative primal error e_b for SPDHG using b -serial sampling with uniform probabilities (solid) and non-uniform probabilities (dashed) as given by (30). The non-uniform sampling shows overall better results, even though its probabilities were determined for a different model.

convex case, we see that smaller batch sizes b appear to yield better performance, however the computational time for smaller batches is longer.

Figures 8b and 8d show the accuracy of the method over time. We see that the computational time increases with the number of FISTA iterations per epoch. In general, the best batch size b is determined by accuracy over time, which depends on the number of FISTA iterations we choose to implement. For a fixed number of FISTA iterations per epoch, the results suggests the performance is still arguably better for lower values of b , even when it takes more time per epoch. However, for fixed number of FISTA iterations per iteration of SPDHG, it is not clear a priori which batch-size b yields faster performance.

Using the parameters from Table 1 we can also compare the performance of uniform

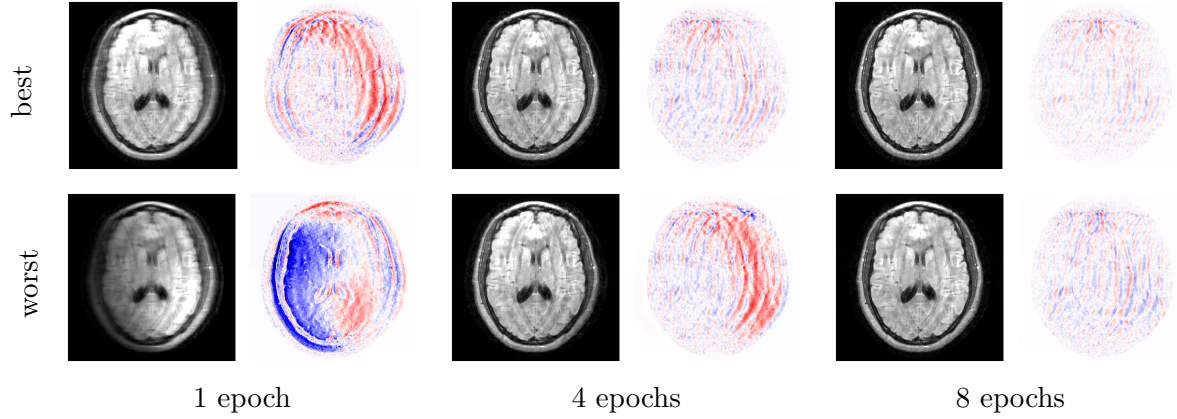


Figure 11: **MRI-TV reconstruction with the best and worst possible sampling.** Reconstructed image $|x^k|$ and real error $\text{Re}(x^k - \hat{x})$, obtained using SPDHG with the b -serial sampling and partitions suggested in Figure 5. We use uniform serial sampling on $b = 1$ as the best sampling (top) and uniform b -serial sampling with $b = 3$ and with the worst partition as the worst possible sampling (bottom). Performance of SPDHG seems improved by the proposed “best” sampling, even if it was determined for a different model.

b -serial and uniform b -nice in Figure 9. The uniform b -serial sampling seems to perform better than uniform b -nice sampling for the case $b = 1$ and $b = 3$. For the other cases the difference is not that clear, even when we use the “best” partition \mathbf{P}_{us}^{best} from last section for b -serial sampling.

Indeed, the uniform b -serial sampling used in Figures 6 to 11 use the “best” partitions suggested from Figure 4 for each b . In contrast with the previous strongly convex model, here we do not have theoretical convergence rates to determine what is the best partition, however we still use the best partitions (38) from last section as candidates for our TV model. Furthermore, we can use the optimal probabilities from last section to implement a non-uniform (not necessarily “optimized”) b -serial sampling. Figure 10 shows the results of using b -serial sampling with uniform and non-uniform probabilities p_i , where the non-uniform probabilities are determined by the strongly convex model from the last section. In both cases, we use the same values γ_b for uniform b -serial sampling from Table 1. Clearly, the results from using the non-uniform probabilities are better, even when these probabilities were determined using an entirely different model. As before, the comparison is trivial for the case $b = n$.

Similarly to last section, we can test SPDHG with the best and worst samplings from the strongly convex model. Figure 11 shows the performance of SPDHG using these two samplings, as described in Figure 5. The proposed “best” sampling also improves performance in this case, even when determined by the strongly convex model.

All these results suggest that the right choice of sampling, which depends strongly on the numerical properties of the operators \tilde{A}_j , may be governed by physical properties of the electromagnetic coils such as their position, as suggested in Figure 3.

6. Conclusions and Discussion

We have closed a gap in the convergence analysis of SPDHG by extending its convergence guarantees to general separable Hilbert spaces and arbitrary sampling. We give a concrete strategy to find parameters that satisfy the required step size condition for all possible random samplings. For several specific random samplings, it is possible to determine theoretically optimal step size parameters. We put these samplings to test using applications to parallel MRI reconstruction.

Our experiments show that the choice of step size parameters directly affects the convergence of the algorithm. Furthermore, the choice of random sampling also strongly influences the performance through several important factors such as whether the indices are chosen independently or grouped into batches (b -nice or b -serial), the partition that defines the batches (e.g. equidistant, consecutive), the probability with which we sample the batches (e.g. uniform, optimized), and the batch size.

For b -serial sampling, we point out the different ways in which a set can be partitioned into batches. For samplings of fixed batch size, we show that choosing a convenient partition to sample from yields much better performance than the many other possible partitions. Empirically, the spatial location of the coils that define the subsets of this best partition motivate the intuitive notion that coils that are closer together correspond to more correlated forward operators A_i , and hence should not be grouped together in the same batch, as that may yield worse step size parameters.

Finally, partitioning the dual variable into smaller subsets and sampling one at a time can be significantly more efficient than taking larger subsets every iteration. This is the case for the L^2 model with optimal b -serial sampling. For the TV model, the best value of b depends strongly on how the FISTA subroutine is implemented within the SPDHG algorithm. For b -nice sampling, in contrast, performance seems to remain consistent across batch size.

In general, our experiments suggest that random samplings perform better than the original deterministic method, b -serial sampling is often better than b -nice sampling, and that there always exist an optimal batch size and partition for every type of sampling. In the strongly convex case, sampling with optimal probabilities significantly outperforms all other sampling strategies.

Acknowledgments

MJE and CD acknowledge support from the EPSRC (EP/S026045/1). MJE is also supported by EPSRC (EP/T026693/1), the Faraday Institution (EP/T007745/1) and the Leverhulme Trust (ECF-2019-478). EBG acknowledges the Mexican Council of Science and Technology (CONACyT).

References

- [1] Jonas Adler, Holger Kohr, and Ozan Öktem. Operator discretization library (odl), January 2017.

- [2] Ahmet Alacaoglu, Olivier Fercoq, and Volkan Cevher. On the convergence of stochastic primal-dual hybrid gradient. *SIAM Journal on Optimization*, 32(2):1288–1318, 2022.
- [3] Heinz H Bauschke, Patrick L Combettes, et al. *Convex analysis and monotone operator theory in Hilbert spaces*, volume 408. Springer, 2011.
- [4] Amir Beck and Marc Teboulle. A fast iterative shrinkage-thresholding algorithm for linear inverse problems. *SIAM Journal on Imaging Sciences*, 2(1):183–202, 2009.
- [5] Bernhard E Boser, Isabelle M Guyon, and Vladimir N Vapnik. A training algorithm for optimal margin classifiers. In *Proceedings of the fifth annual workshop on Computational learning theory*, pages 144–152, 1992.
- [6] Kristian Bredies and Dirk Lorenz. *Mathematical Image Processing*. Springer, 2018.
- [7] Volkan Cevher, Stephen Becker, and Mark Schmidt. Convex optimization for big data: Scalable, randomized, and parallel algorithms for big data analytics. *IEEE Signal Processing Magazine*, 31(5):32–43, 2014.
- [8] Antonin Chambolle, Matthias J Ehrhardt, Peter Richtárik, and Carola-Bibiane Schönlieb. Stochastic primal-dual hybrid gradient algorithm with arbitrary sampling and imaging applications. *SIAM Journal on Optimization*, 28(4):2783–2808, 2018.
- [9] Antonin Chambolle and Thomas Pock. A first-order primal-dual algorithm for convex problems with applications to imaging. *Journal of mathematical imaging and vision*, 40(1):120–145, 2011.
- [10] Antonin Chambolle and Thomas Pock. An introduction to continuous optimization for imaging. *Acta Numerica*, 25:161–319, 2016.
- [11] Subhasis Chaudhuri. *Super-resolution imaging*, volume 632. Springer Science & Business Media, 2001.
- [12] Patrick L Combettes and Jean-Christophe Pesquet. Stochastic quasi-Fejér block-coordinate fixed point iterations. *SIAM Journal on Optimization*, 25(2):1221–1248, 2015.
- [13] Matthias J Ehrhardt, Pawel Markiewicz, and Carola-Bibiane Schönlieb. Faster PET reconstruction with non-smooth priors by randomization and preconditioning. *Physics in Medicine & Biology*, 64(22):225019, 2019.
- [14] Ernie Esser, Xiaoqun Zhang, and Tony F Chan. A general framework for a class of first order primal-dual algorithms for convex optimization in imaging science. *SIAM Journal on Imaging Sciences*, 3(4):1015–1046, 2010.
- [15] Olivier Fercoq, Ahmet Alacaoglu, Ion Necoara, and Volkan Cevher. Almost surely constrained convex optimization. In *International Conference on Machine Learning*, pages 1910–1919. PMLR, 2019.
- [16] Olivier Fercoq and Pascal Bianchi. A coordinate-descent primal-dual algorithm with large step size and possibly nonseparable functions. *SIAM Journal on Optimization*, 29(1):100–134, 2019.
- [17] Jeffrey A Fessler. Optimization methods for magnetic resonance image reconstruction: Key models and optimization algorithms. *IEEE Signal Processing Magazine*, 37(1):33–40, 2020.
- [18] Xiang Gao, Yang-Yang Xu, and Shu-Zhong Zhang. Randomized primal-dual proximal block coordinate updates. *Journal of the Operations Research Society of China*, 7(2):205–250, 2019.
- [19] Eric B Gutiérrez, Claire Delplancke, and Matthias J Ehrhardt. Convergence properties of a randomized primal-dual algorithm with applications to parallel mri. In *International Conference on Scale Space and Variational Methods in Computer Vision*, pages 254–266. Springer, 2021.
- [20] William Hager, Cuong Ngo, Maryam Yashtini, and Hong-Chao Zhang. An alternating direction approximate newton algorithm for ill-conditioned inverse problems with application to parallel mri. *Journal of the Operations Research Society of China*, 3(2):139–162, 2015.
- [21] Thorsten Hohage and Carolin Homann. A generalization of the chambolle-pock algorithm to banach spaces with applications to inverse problems. *arXiv preprint arXiv:1412.0126*, 2014.
- [22] Florian Knoll, Jure Zbontar, Anuroop Sriram, Matthew J Muckley, Mary Bruno, Aaron Defazio, Marc Parente, Krzysztof J Geras, Joe Katsnelson, Hersh Chandarana, et al. fastmri: A publicly available raw k-space and dicom dataset of knee images for accelerated mr image reconstruction using machine learning. *Radiology: Artificial intelligence*, 2(1), 2020.

- [23] Puya Latafat, Nikolaos M Freris, and Panagiotis Patrinos. A new randomized block-coordinate primal-dual proximal algorithm for distributed optimization. *IEEE Transactions on Automatic Control*, 64(10):4050–4065, 2019.
- [24] Frank Ong, Jonathan Martin, Will Grissom, Siddharth Srinivasan, Kevin M Johnson, Chris Huynh, Arjun Desai, Zhitao Li, Jon Tamir, Chris Sandino, Efrat Shimron, David Zeng, and Nikolai Mickevicius. mikgroup/sigpy: Minor release to trigger Zenodo for DOI. (v0.1.24). *Zenodo*, 2022
<https://doi.org/10.5281/zenodo.5893788>.
- [25] Frank Ong, Xucheng Zhu, Joseph Y Cheng, Kevin M Johnson, Peder EZ Larson, Shreyas S Vasanaawala, and Michael Lustig. Extreme mri: Large-scale volumetric dynamic imaging from continuous non-gated acquisitions. *Magnetic resonance in medicine*, 84(4):1763–1780, 2020.
- [26] Andrei Patrascu and Ion Necoara. Nonasymptotic convergence of stochastic proximal point methods for constrained convex optimization. *The Journal of Machine Learning Research*, 18(1):7204–7245, 2017.
- [27] T. Pock, D. Cremers, H. Bischof, and A. Chambolle. A algorithm for minimizing the Mumford-Shah functional. In *2009 IEEE 12th International Conference on Computer Vision*, pages 1133–1140, 2009.
- [28] Thomas Pock and Antonin Chambolle. Diagonal preconditioning for first order primal-dual algorithms in convex optimization. In *2011 International Conference on Computer Vision*, pages 1762–1769. IEEE, 2011.
- [29] Klaas P Pruessmann. Encoding and reconstruction in parallel mri. *NMR in Biomedicine: An International Journal Devoted to the Development and Application of Magnetic Resonance In vivo*, 19(3):288–299, 2006.
- [30] Klaas P Pruessmann, Markus Weiger, Markus B Scheidegger, and Peter Boesiger. Sense: sensitivity encoding for fast mri. *Magnetic Resonance in Medicine: An Official Journal of the International Society for Magnetic Resonance in Medicine*, 42(5):952–962, 1999.
- [31] Zheng Qu, Peter Richtárik, and Tong Zhang. Quartz: Randomized dual coordinate ascent with arbitrary sampling. *Advances in neural information processing systems*, 28, 2015.
- [32] Herbert Robbins and David Siegmund. A convergence theorem for non negative almost supermartingales and some applications. In *Optimizing methods in statistics*, pages 233–257. Elsevier, 1971.
- [33] Leonid I Rudin, Stanley Osher, and Emad Fatemi. Nonlinear total variation based noise removal algorithms. *Physica D: nonlinear phenomena*, 60(1-4):259–268, 1992.
- [34] J Sakurai and J Napolitano. Modern quantum mechanics. 2-nd edition. *Person New International edition*, 2014.
- [35] Georg Schramm and Martin Holler. Fast and memory-efficient reconstruction of sparse poisson data in listmode with non-smooth priors with application to time-of-flight pet. *Physics in Medicine & Biology*, 2022.
- [36] Shai Shalev-Shwartz and Tong Zhang. Stochastic dual coordinate ascent methods for regularized loss minimization. *Journal of Machine Learning Research*, 14(Feb):567–599, 2013.
- [37] Martin Vetterli and Jelena Kovacevic. *Wavelets and subband coding*. Prentice-hall, 1995.
- [38] Jure Zbontar, Florian Knoll, Anuroop Sriram, Tullie Murrell, Zhengnan Huang, Matthew J Muckley, Aaron Defazio, Ruben Stern, Patricia Johnson, Mary Bruno, et al. fastMRI: An open dataset and benchmarks for accelerated MRI. *arXiv preprint arXiv:1811.08839*, 2018.
- [39] Yuchen Zhang and Lin Xiao. Stochastic primal-dual coordinate method for regularized empirical risk minimization. *The Journal of Machine Learning Research*, 18(1):2939–2980, 2017.